



A FVCOM study of the potential coastal flooding in apponagansett bay and clarks cove, Dartmouth Town (MA)

Zhuo Zhang^{1,2} · Changsheng Chen³ · Zhiyao Song^{1,2} · Dong Zhang^{1,2} · Di Hu^{1,2} · Fei Guo^{1,2}

Received: 21 November 2018 / Accepted: 4 June 2020 / Published online: 17 June 2020
© Springer Nature B.V. 2020

Abstract

A high-resolution Finite-Volume Coastal Ocean Model (FVCOM) inundation model has been developed for Dartmouth Town near Apponagansett Bay and Clarks Cove. Series of modeling experiments were conducted for the purpose of: (1) Assess the potential impacts of the climate-induced Sea Level Rise (SLR) on the storm-induced coastal inundation in Dartmouth Town; (2) Compare the current patterns, wave fields and surge distributions under different dynamic forces including winds in different directions and wave-current interaction; (3) Evaluate the impact of the bank on the flooding protection. Results show that under the hundred-year nor'easter storm condition, the climate-induced SLR could significantly enlarge possible flooding areas with the percent area enlargement of approximately 60% per foot of SLR. The directions of wind essentially determine the feature of the current patterns, wave and surge distributions. The northeasterly and easterly winds mainly threaten the western coast of the bay and the estuarine areas, and the southerly and southeasterly winds endanger the regions around the inner part of the bay. Wave-current interaction can change the current pattern nearshore, including formation of eddies and narrow alongshore currents, greatly enhancing the strength and complexity of the currents near the mouth of the bay. In addition, wave-induced surge tends to accumulate in the bay and near the estuary and coastal regions. The bank blocks a large amount of flooding current and waves into the bay and improves the local current and wave condition effectively near the mouth and in the bay.

Keywords Coastal flooding · Inundation · Surge · Wave-current interaction · Sea level rise · Storm

✉ Zhuo Zhang
mercury1214@126.com

¹ Key Laboratory of Virtual Geographic Environment (Nanjing Normal University), Ministry of Education, Nanjing 210023, China

² Jiangsu Center for Collaborative Innovation in Geographical Information Resource Development and Application, Nanjing 210023, China

³ School for Marine Science and Technology, University of Massachusetts-Dartmouth, New Bedford, MA 02744, USA

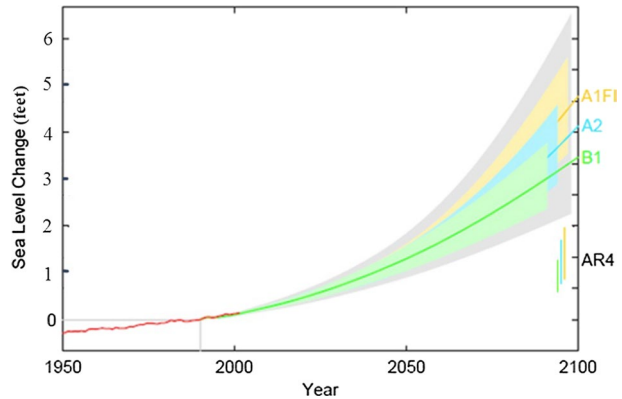
1 Introduction

Coastal inundation is defined as flooding of normally dry land caused generally by some combination of heavy rains, high river discharge, tides, wind waves, storm surges, and tsunami wave trains. Hurricanes (tropical cyclones) and nor'easters (extratropical cyclones) are two major storm systems for flood risk along the Massachusetts coast (Zhang et al. 2000). Serious coastal inundation usually happens when combined wind waves and storm surges coincide with high tides (Bernier and Thompson 2006; Chen et al. 2013; Beardsley et al. 2013). For example, the August 18–19 1991 Hurricane Bob-generated strong winds (>40 m/s), high storm surges, and heavy rains caused extensive damage over New England, with a total loss of \$1.5 billion in economy (Mayfield 1992; Vallee and Dion 2005). Hurricane Sandy swept over the US northeast region on October 28–29 2012, with wind gusts above 37 m/s over Cape Cod and Buzzards Bay, MA. With its unusual merge with an air frontal system, “Superstorm Sandy” caused serious flooding along the New England coast and led to an economic loss of ~\$75 billion, including property damage, widespread power outages, subway shutdown in cities, and the closing of many businesses in the region (Blake et al. 2013, USA Today-October 30 2012).

In Massachusetts, coastal inundation and damage are frequently caused by nor'easters and much less frequently by tropical cyclones. The October 1991 extratropical cyclone (“Perfect Storm” or “Halloween Nor'easter of 1991”) produced strong winds (peak gusts above 27 m/s) and 8-m waves during high tides (1.2 m above normal), causing serious coastal flooding in eastern Massachusetts (esp. Cape Ann to Nantucket), with damage of ~\$100 M (seven counties declared Federal Disaster counties) (McCown 2008). The December 27 2010 nor'easter (Freedman 2013) produced sustained peak winds above 23 m/s and 6-m waves above high tides off Scituate, a coastal town located about 25 km southeast of Boston. The combination of high wind-driven along-shore currents and waves peaking near high tide caused serious flooding on both the North Shore (e.g. Rockport) and South Shore (e.g. Scituate) (Beardsley et al. 2013). Many houses lost power and were damaged, and parts of the primary sea wall were breached. The recent February 8–9 2013 nor'easter (“Blizzard of 2013”), a super winter storm formed by the merger of a warm moist Mid-Atlantic low and a cold northeast low, caused a snowfall of >25 inches (0.6 m) and a storm surge of ~1.3–1.5 m in the Boston area (Freedman 2013). The governor of Massachusetts declared a “state of emergency” for the blizzard (CBS News-February 8, 2013), with an initial estimate of coastal and property damage and economic loss greater than past nor'easter events.

According to the Intergovernmental Panel on Climate Change (IPCC) 4th Assessment Report (IPCC 2007), climate change shows a tendency that future tropical and extratropical storms will be more intense and storm-produced coastal inundation will likely worsen as a result of rapid sea level rise (SLR) in tropic and extratropical regions of the North Atlantic Ocean. SLR will continue as thermal expansion due to climate warming, rapid melting of ice sheets in the Arctic and Antarctic Oceans (Pritchard et al. 2012; Hellmer et al. 2012), and melting glaciers. Projected SLR estimated from global temperature warming will be in the range of 0.2–0.5 m at 2050 and up to 1.0–2.0 m at the end of this century (Fig. 1) (Sallenger et al. 2012). This value could be much higher due to more rapid melting of ice sheets in summer in Greenland and west Antarctic ice sheets (Rahmstorf 2010). A recent assessment of the effect of SLR on predicted changes in the intensity and paths of hurricanes in the North Atlantic shows that New York City will experience significantly larger storm surges (Lin et al. 2012).

Fig. 1 Projection of sea-level rise over 1995–2100 based on the IPCC temperature projection for three emission scenarios (B1, A2 and A1F1) (IPCC 2007). Figure is downloaded from Vermeer and Rahmstorf (2009)



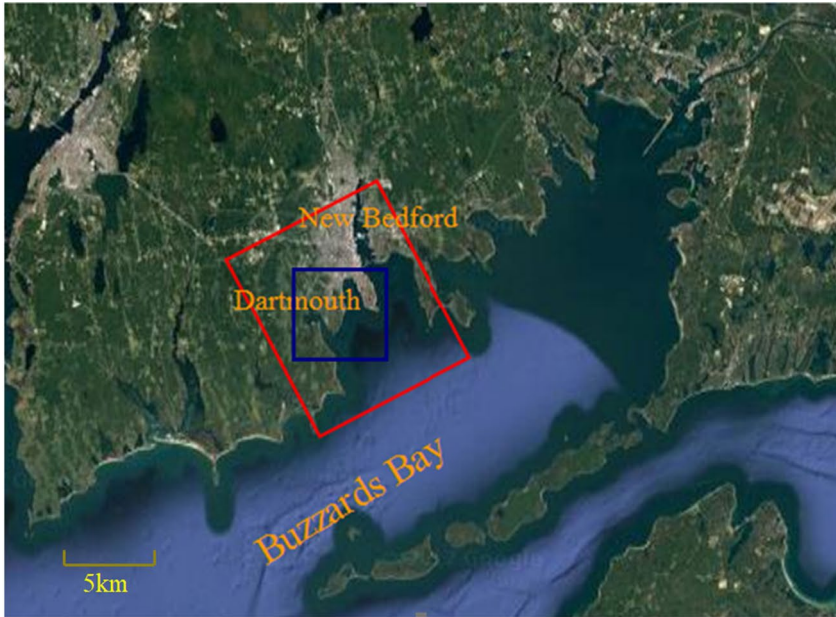
Wave-current interaction plays a significant role in coastal inundation. However, most previous inundation models did not consider wave-current interaction, such as Peng et al. (2006) and Oey (2006). Although some models included wave-current interaction, they were one-way coupled, with inclusion of the wave radiation stress into the current model and without the current's effect on waves such as Nielson and Apelt (2003) and Castelle et al. (2006). Xie et al. (2008) developed a two-way and dynamic inundation model by coupling POM model and SWAN wave model. Nevertheless, the structured grid restricted the model to match the complicated coastlines and capture small scale features in topography. Moreover, the majority of previous efforts to characterize potential coastal impacts of climate change focused primarily on long-term SLR with a static water level, and few comprehensively accounted for dynamic physical drivers of a storm-inundation event, such as storm, tide, waves and surges, which are not simply superposed, but are non-linear interactions with each other.

For better assessing the effect of the wave-current interaction on surge at different tidal phases, and further predicting consequences carried by the flooding under extreme weather and climate change in Dartmouth Town, we have developed a high-resolution coastal inundation forecast model based on FVCOM (Chen et al. 2003, 2011). We applied an unstructured-grid finite-volume version of the SWAN surface wave model (named "FVCOM-SWAVE") and coupled it with FVCOM to conduct two-way wave-current interaction simulations (Qi et al. 2009). The pattern of current, waves and potential inundation area around Apponagansett Bay and Clarks Cove under various sea level rises (SLRs) and extreme high-speed winds has been assessed.

The following sections are organized as follows: The study area is introduced in Sect. 2 section; The method including the model introduction and design of numerical experiments are described in Sect.3 section; The model results under various conditions are presented in Sect.4 section. The separate effect of wind, waves and bank is discussed in Sect. 5 section and some conclusions are drawn in Sect.6 section.

2 Study areas

The Apponagansett Bay and Clarks Cove is located on the western coast of Buzzard Bay (Fig. 2). This region was frequently influenced by storm-induced coastal inundation. The National Oceanic and Atmospheric Administration (NOAA) National Weather Service



(a)



(b)

Fig. 2 Coastal areas around Buzzards Bay **a** and the zoom-in views of study area located in the blue box **(b)**. The region marked by a red color box is the computational domain of the DTC-FVCOM

(NWS) Weather Forecast Offices (WFOs) in Taunton (MA) has identified 23 other coastal sites in Massachusetts that are “particularly vulnerable to extratropical flooding” and ten sites are in Buzzards Bay that are “most vulnerable” to extreme storm surge during hurricanes. Dartmouth is a coastal town in New England and was the first area of southeastern Massachusetts settled. It is the third largest town by area in Massachusetts. Surrounding the town, Apponagansett Bay and Clarks Cove have a significant influence on local inundation. With climate change scenarios predicting stronger storms and rising sea level, coastal flooding-induced hazards will directly affect local safety, marine and public activities, the coastal environment and economy.

3 Methods

3.1 A high-resolution DTC-FVCOM

Built on the success in establishing an “end-to-end” coastal inundation forecast model system under the framework of the Northeast Coastal Ocean forecast System (NECOFS), we have developed a high-resolution, subdomain coastal inundation model for the western Buzzard Bay coast, with the computational domain covering Apponagansett Bay and Clarks Cove (Fig. 2). This subdomain inundation model was constructed using the unstructured grid, Finite Volume Community Ocean Model (FVCOM), and named the Dartmouth Town Coastal FVCOM (abbreviated as “DTC-FVCOM”). The DTC-FVCOM was a coupled surface wave (FVCOM-SWAVE)/3-D ocean circulation model (FVCOM) system with built-in flooding/drying capability. FVCOM-SWAVE was implemented into FVCOM through the 3-D radiation stress approach (Mellor 2003, 2008; Warner et al. 2008). FVCOM is a prognostic, unstructured-grid, Finite-Volume, free-surface, 3-D primitive equation Community Ocean Model developed originally by Chen et al. (2003) and has been improved by a team of UMASSD and WHOI researchers (Chen et al. 2003, 2006a, b, 2013). The equations are cast in a generalized terrain-following coordinate system with spatially variable vertical distribution (Pieterzak et al. 2002). The spatial fluxes of momentum are discretized using a second-order accurate finite-volume method (Kobayashi et al. 1999). A flux formulation for scalars (e.g. temperature, salinity) is used in conjunction with a vertical velocity adjustment to enforce exact local and global conservation of the scalar quantities. A Smagorinsky formulation (Smagorinsky 1963) is used to parameterize the horizontal diffusion and turbulent vertical mixing is calculated using the General Ocean Turbulence Model (GOTM) libraries (Burchard 2002), with the 2.5 level (Mellor-Yamada 1982) turbulence model used as the default. The ability of FVCOM to accurately solve scalar conservation equations combined with the topological flexibility provided by unstructured meshes makes it ideally suited for environmental prediction and interdisciplinary applications in coastal regions (see examples on <http://fvcom.smast.umassd.edu>).

3.1.1 Model grids and bathymetry

The computational domain of the DTC-FVCOM was configured with the unstructured triangles with a total node number of 44,956 and a total cell number of 89,717. The horizontal resolution was up to ~10 m (Fig. 3). Six σ -levels (5 layers) with a uniform thickness was specified in the vertical, which produced a vertical resolution of 4 m on the 40-m isobath and up to ~0.5 m on the 5-m isobaths.

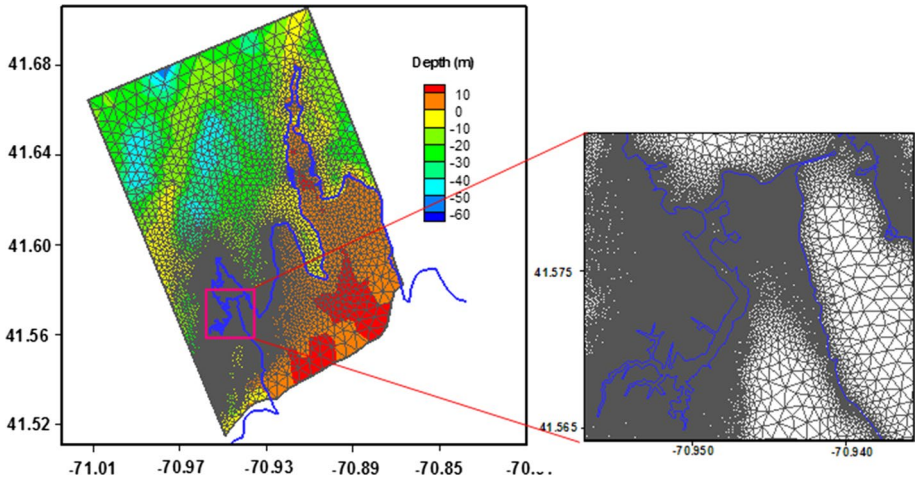


Fig. 3 The unstructured triangular grid used for the DTC-FVCOM. The color image illustrated the water depth (positive for the water and negative for the land)

An effort was made to collect the high-resolution bathymetry in the Dartmouth coastal region. The bathymetry used in the DTC-FVCOM were from the two sources. The Dartmouth Town provided us with the 1.0-m resolution USGS light detection and ranging (LiDAR) bathymetry data, which covered the Apponagansett Bay and Clarks Cover regions. In the area where the LiDAR was not available, we used the shuttle radar topography mission (STRM) data, which had a horizontal resolution of ~ 30 m.

3.1.2 Forcing and boundary conditions

The DTC-FVCOM was fully current-wave coupled hydrodynamic model driven by the surface wind stress with lateral boundary conditions specified using the tidal and non-tidal elevations plus significant wave height, direction and peak frequency. There was neither a tidal gauge nor a meteorological surface buoy for monitoring the water elevation, wind and surface waves in Apponagansett Bay and Clarks Cove. The tidal elevations on the boundary, the wind forcing at the sea surface, and significant wave height/direction/peak frequency were provided by the reanalysis results of NECOFS.

The hundred-year storm wind was determined by the statistical storm analysis of the wind field produced by the meso-scale weather model (named “WRF”) in NECOFS. The storm was defined according to the magnitude and duration of the wind stress. When the local wind exceeded 0.2 Pa (25 mph) and lasted at least for 6 h, we defined it as a storm (Butman et al. 2008). Over the 39-year period from 1978 to 2016, there were a total of 364 storms that struck Buzzard Bay. The extreme wind speed for a 100-year storm was 24 m/s (53.7 mph) (Fig. 4), blowing predominantly from the northeast direction. A constant wind speed of 24 m/s, which represented for wind intensity of a hundred-year storm, was specified for the numerical simulation.

To assess the impact of sea level rise on possible maximum flooding, we considered a spring tidal condition. The NECOFS product included the hourly water elevation over the 39-year period from 1978 to 2016. We selected a point closed to Apponagansett Bay and conducted the harmonic analysis for the water elevation. The resulting magnitude of the

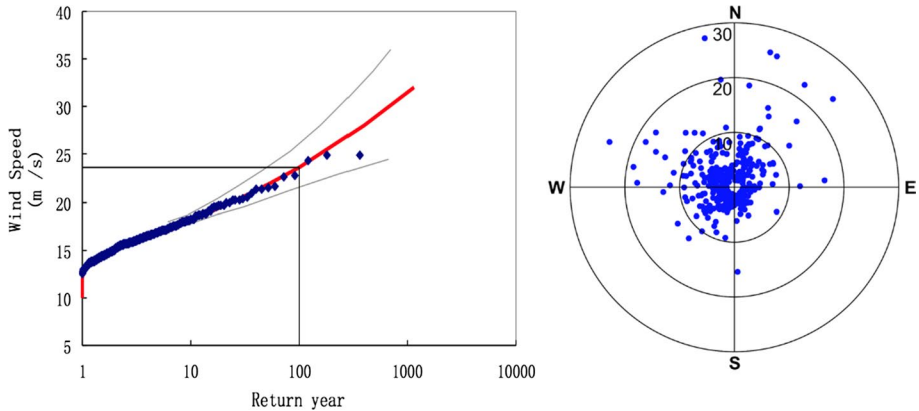


Fig. 4 Left: Wind speed versus the storm return year. Dots: storm data samples; red curve: the extremal wind curve; grey curves: the 95% confidence interval. Right: Distributions of wind directions for individual storms. Labels “E, S, W and N” present the east, south, west and north directions, respectively. The wind direction was defined as the direction at which the wind blew from. The numbers on each axis were the wind speed. Analysis was done with 364 storm samples

tidal elevation in Apponagansett Bay during a spring tide cycle was 0.65 m (2.13 feet). The tidal forcing on the boundary was specified using a semi-diurnal M_2 tidal constituent with a magnitude of 0.65 m, which considered the maximum tidal elevation occurring during the spring tidal cycle.

The significant wave height and peak frequency were estimated based on the NECOFS-predicted surface waves in Buzzard Bay. In August 1991, Buzzard Bay was attacked by Hurricane Bob. Based on our simulation results, we found that the maximum surface wave height could reach 3.0 m (m), with a peak period of 10 s (s) in Buzzard Bay. To take the extreme condition into account, we specified a significant wave height of 3.0 m at a peak period of 10 s as forcing of surface waves on the boundary. In all simulations with inclusion of surface waves, the surface wave propagated onshore.

3.2 Design of numerical experiments

To provide a more objective assessment on the impact of climate-induced rise level rise on the potential coastal inundation in Apponagansett Bay and Clarks Cove, we conducted the experiments under different physical conditions. A total of 22 cases were selected to run the model, with the detailed descriptions are summarized in Table 1.

The first 6 experiments focus on various wind directions which may significantly affect the flooding and inundation. The first experiment (Case 1) was made for the hundred-year storm case from statistical analysis with no sea level rise (SLR). In this case, a northeasterly wind was specified. To ensure that the model capture the worst flooding situation, we also ran the model with the same wind amplitude but different wind directions. Case 2–6 represented for experiments with northerly, northwesterly, easterly, southerly and southeasterly winds. We found that for given same condition of tidal and wave forcings on the boundary, the southeasterly wind could cause relatively larger flooding and inundation surrounding Apponagansett Bay. Although in the historic wind data, the occurrence frequency of southeasterly wind was very low, it might be possible when a hurricane attacks Buzzard

Table 1 The list of the forcing used in the 13 experiments

Fully wave-current coupled experiments with no SLR					
Case	Winds	Waves	Tides	SLR (feet)	Description
1	Yes	Yes	Yes	0	Northeasterly wind
2	Yes	Yes	Yes	0	Northerly wind
3	Yes	Yes	Yes	0	Northwesterly wind
4	Yes	Yes	Yes	0	Easterly wind
5	Yes	Yes	Yes	0	Southerly wind
6	Yes	Yes	Yes	0	Southeasterly wind
Fully wave-current coupled experiments with SLR					
Case	Winds	Waves	Tides	SLR (feet)	Description
7	Yes	Yes	Yes	1.0	Northeasterly wind
8	Yes	Yes	Yes	2.0	Northeasterly wind
9	Yes	Yes	Yes	3.0	Northeasterly wind
10	Yes	Yes	Yes	4.0	Northeasterly wind
11	Yes	Yes	Yes	5.0	Northeasterly wind
12	Yes	Yes	Yes	6.0	Northeasterly wind
13	Yes	Yes	Yes	1.0	Southeasterly wind
14	Yes	Yes	Yes	2.0	Southeasterly wind
15	Yes	Yes	Yes	3.0	Southeasterly wind
16	Yes	Yes	Yes	4.0	Southeasterly wind
17	Yes	Yes	Yes	5.0	Southeasterly wind
18	Yes	Yes	Yes	6.0	Southeasterly wind
Process-oriented experiments					
Case	Winds	Waves	Tides	SLR	Description
19	No	Yes	No	0	Only waves
20	No	No	Yes	0	Only tides
21	No	Yes	Yes	0	Tidal and wave, but no wind
22	Yes	No	Yes	0	Tide plus northeasterly wind, but no wave
23	Yes	No	Yes	0	Tide plus southeasterly wind, but no wave

Bay. For this reason, we selected the cases with northeasterly (100-year nor'easter storm) and southeasterly (possible a hurricane) winds as two representatives for our analysis.

Experiments with SLRs were made for the cases with northeasterly and southeasterly winds, respectively. In each case, we re-ran the fully wave-current coupled model with 1.0–6.0 feet of SLR, respectively (Cases 7–12: northeasterly wind; Case 13–18: southeasterly wind). These cases were designed to assess the impact of climate change-induced sea level rise on the possible future storm-induced flooding in the region.

The contribution of the separate forcing can hardly be assessed in measurements but easily estimated in numerical simulation. To evaluate the model performance under the different forcing conditions, we made 4 additional experiments to run the model with only wave forcing (Case 19), only tidal forcing (Case 20), tidal plus wave forcing (Case 21) and wind plus tidal forcing (Case 22), respectively.

All experiments were made over a two-day period. The tidal elevation reached an equilibrium state after half a day, while the wind and wave forcing was spin up over a tidal cycle. The maximum flooding occurred at the high tide after spin up time. The model output at the second-high tide on the second model-run day were used to draw the flooding map.

4 Model results

4.1 Inundation maps

The model-predicted, storm-induced flooding is illustrated using the inundation map in Fig. 5, with zoom-in views on two selected areas along the southeastern coast of Apponagansett Bay and the western coast of Clarks Cove in Figs. 7, 8, respectively.

For the case with the northeasterly wind, under the same hundred-year nor'easter storm condition, the climate-induced SLR could significantly enlarge possible flooding. In this case, the percentage rate of the area enlargement is approximately 60% per foot of SLR (Table 2; Fig. 6). When the SLR reaches 6 feet, the flooding area could enlarge by 506% relative to the flooding area with 0.0 feet of SLR. This enlargement rate is much higher than the linear increase rate found for the cases with 1.0–5.0 feet of SLR. Compared with the case with northeasterly wind, the southeasterly wind produced a relatively larger flooding area: 8% larger. In this case, the percentage rate of the area enlargement is around 48% per foot of SLR (Table 3; Fig. 6). This suggests that for the given intensity of an extratropical (nor'easter) or tropical (hurricane) storm, the impact of SLR is higher in the case with northeasterly wind.

The enlarged view of possible flooding area along the southeastern coast of Padanaram is given in Fig. 7. Given the same intensity of a hundred-year storm, flooding along the

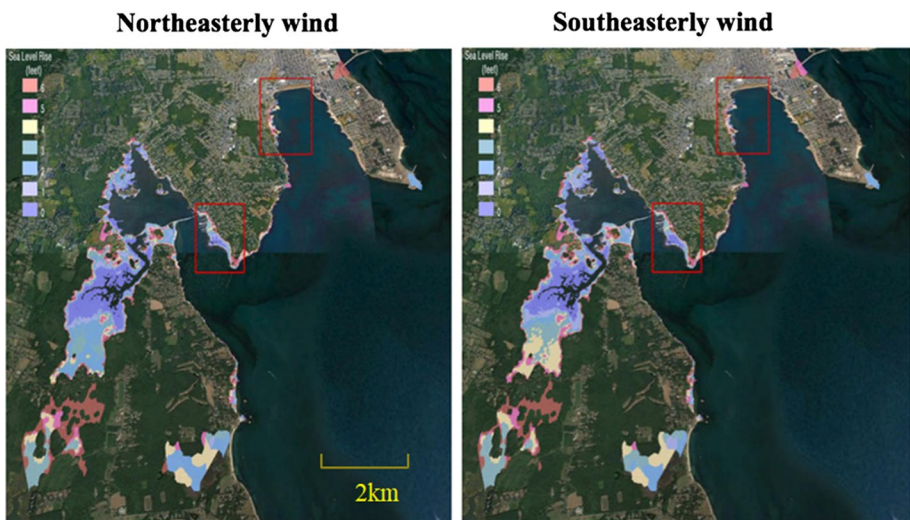


Fig. 5 The inundation map of possible flooding in Apponagansett Bay and Clarks Cove for the cases with 0.0–6.0 feet of SLR under the northeasterly (left) and southeasterly (right) wind conditions, respectively. The red rectangle box in the right panel is the area where the zoom-in map was drawn

Table 2 Possible flooding areas for the case with northeasterly wind

Case	Flooding areas (km ²)	Enlargement (%)	SLR	Description
1	1.34	0	0.0	Northeasterly wind
7	2.14	60	1.0	Northeasterly wind
8	3.07	129	2.0	Northeasterly wind
9	3.69	175	3.0	Northeasterly wind
10	4.72	252	4.0	Northeasterly wind
11	5.62	319	5.0	Northeasterly wind
12	6.78	506	6.0	Northeasterly wind

The area enlargement rate is estimated relative to the flooding area with 0.0 feet of SLR

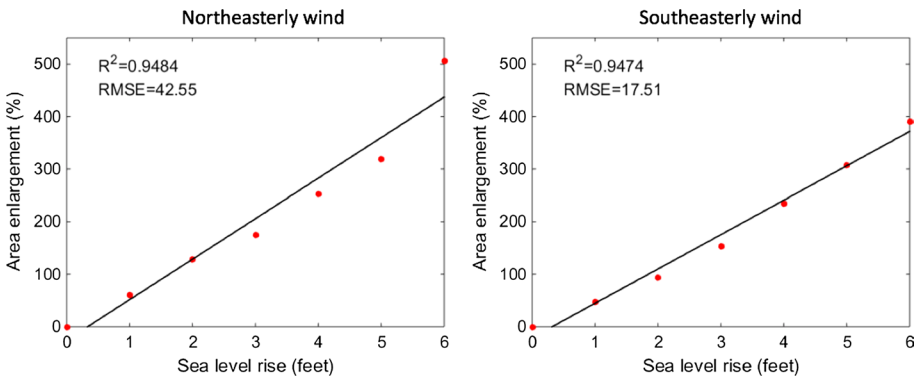


Fig. 6 Percentage rate of flooding-area enlargement with the SLR for the cases with northeasterly (left) and southeasterly (right) winds

Table 3 Possible flooding areas for the case with southeasterly wind

Case	Flood-ing areas (km ²)	Enlargement (%)	SLR (feet)	Description
6	1.45	0	0.0	Southeasterly wind
13	2.14	48	1.0	Southeasterly wind
14	2.81	94	2.0	Southeasterly wind
15	3.69	154	3.0	Southeasterly wind
16	4.86	235	4.0	Southeasterly wind
17	5.92	308	5.0	Southeasterly wind
18	7.11	390	6.0	Southeasterly wind

The area enlargement rate is estimated relative to the flooding area with 0.0 feet of SLR

southeastern coast on the south of the Apponagansett Bay bridge was similar in the cases with northeasterly and southeasterly winds. For a worse situation with 6.0 feet of SLR, the water could cross Elm Street in Padanaram, South Dartmouth and houses on the beachside

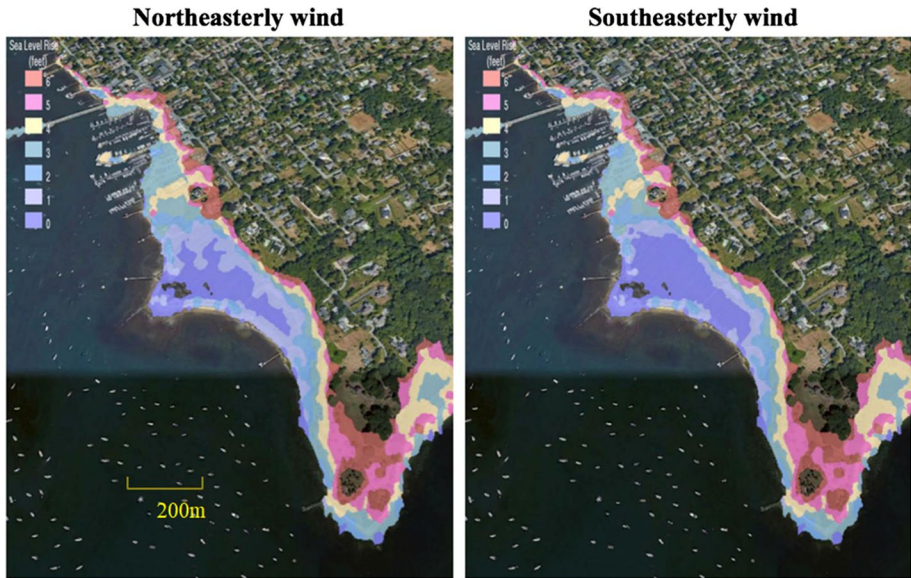


Fig. 7 Enlarged view of possible flooding areas in the Padanaram coast for the cases with 0.0–6.0 feet of SLR under the given northeasterly (left) and southeasterly (right) wind conditions

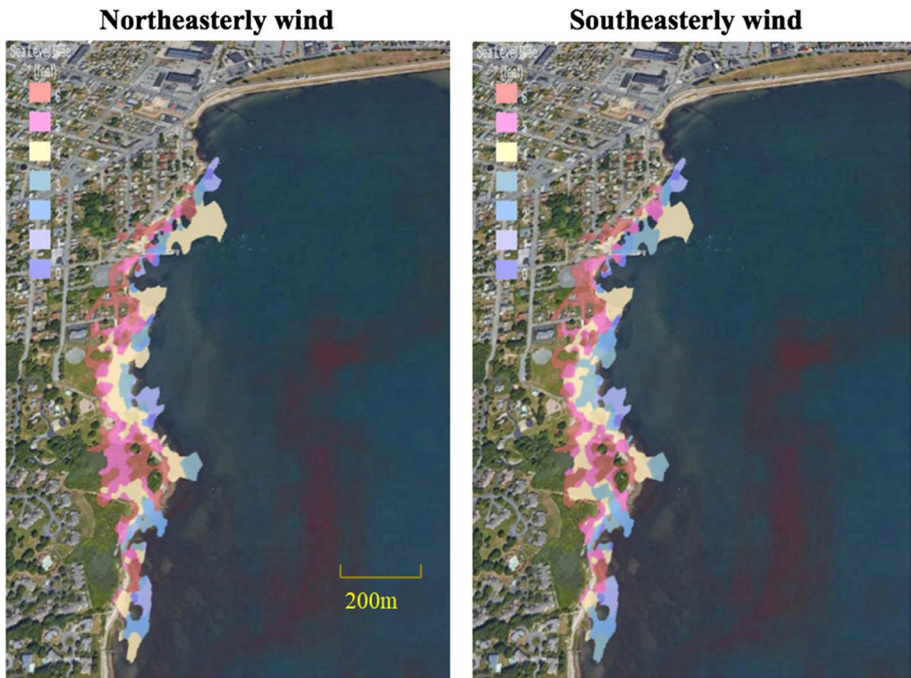


Fig. 8 Enlarged view of possible flooding areas in the Clarks Cove coast or the cases with 0.0–6.0 feet of SLR under the given northeasterly (left) and southeasterly (right) wind conditions

of Ricketson Point could be at risk to be flooded. It should be pointed out here that our estimation did not count the wave runup-induced splashing or overtop, which could be significant and could be intensified with SLR during the southeasterly wind period. The view of possible flooding region can be viewed in the Google Earth map created using the model output (see the deliverable section).

The enlarged view of the possible flooding area along the northern and western coast of Clarks Cove is given in Fig. 8. We can see that the seawall on the northern coast will function well to protect the city from storm-induced flooding, even in the case with 6.0 feet of SLR. However, on the western coast of Clarks Cove, a coast without the seawall, could be significantly influenced by the SLR. For the case with 6.0 feet of SLR, for example, the seawater could cross Padanaram Ave and Marianna Street during both northeasterly and southeasterly wind periods. The flooding could be more worse during the northeasterly wind period.

4.2 Waves

Surface waves were simulated under normal sea level and six SLRs (from 1 to 6 feet) plus northeasterly and southeasterly wind respectively. As shown in Fig. 9, waves propagate from the open sea towards the coastline and damp dramatically along the way under rapid dissipation in the breaker/surf zone. Restricted by coastline geometry and topography in Apponagansett Bay, the major waves are blocked outside the bay by the bank and only small portion of the wave energy can transmit into the bay under normal sea level. Under the given same condition of tidal and wave forcings on the boundary and wind forcing at the sea surface, the surface wave could become much strong as the sea level rises. For the cases with 6.0 feet of SLR, the significant wave height could increase by ~3 feet with more extensive approaching areas. This means that under the same storm condition, we will expect much strong surface waves in the southern area of the Apponagansett Bay on the seaside of the bridge. Moreover, wind influences the wave propagation significantly near offshores, in the bay and inundated areas under SLR. Comparatively, the southeasterly wind driven larger waves in the bay for its longer wind fetch. Overall, the model captures the general characteristic of waves outside and inside the bay well.

4.3 Current

The tidal current process under wave-current interaction is also simulated under the normal sea level and six SLRs (from 1 to 6 feet) plus northeasterly and southeasterly wind respectively. The current pattern in Fig. 10 demonstrates that a two-eddy flow is formed in the southern area: anticyclonic close to the bank and cyclonic in the down southern region. The two-eddy flow is intensified significantly as the SLR reaches 6 feet. These two eddies push the water towards the western coast, which can significantly enhance flooding over that area. Although we did not count the flooding due to the wave runup in our experiments. It is clear that the Apponagansett Bay bridge will face a more serious attack by the storm-induced surface waves as the sea level rises. As a result of the intensification of the surface waves, the current-wave interaction could cause a much strong flow toward the bridge, and hence enhance flooding. The wind direction influences the current pattern more in the bay than outside the bay. Under the southeasterly wind, a cyclonic eddy tends to form in the bay near the bridge, which may threat the eastern region of the bay.

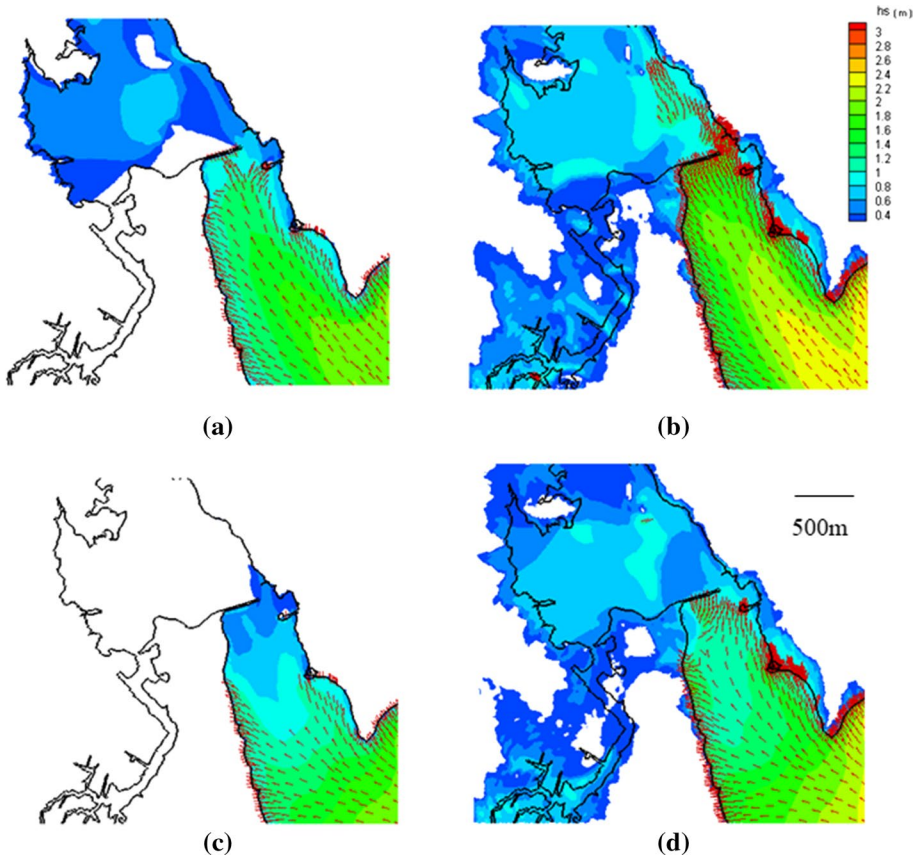


Fig. 9 The wave fields in Apponagansett Bay. The left panels are waves driven by southeasterly (a) and northeasterly winds (c) with no SLR. The right panels are waves under the same wind with a SLR of 6.0 feet in (b) and (d). The color denotes the significant wave height and the vectors denote the wave direction

5 Discussion

5.1 Effect of wind

The depth-averaged current patterns during ebbing under different wind directions are shown in Fig. 11. Firstly, we focus on the current patterns near the mouth of the bay. The current patterns under the northeasterly, the northly and the easterly winds are similar, characteristic of large-scale south-westward current near the mouth of the bay. In contrast, the large-scale current near the mouth turns to north under the south wind. Under southeasterly and northwesterly winds, a more complicated current pattern with cyclonic and anticyclonic eddies is formed. Secondly, turn our focus to the east coastal offshore of Dartmouth featured by a narrow northward alongshore current in Clarks cove. Obviously, this current is not caused by wind because it exist on all wind conditions. However, it is influenced by the winds. Under the northeasterly, northly and northwesterly winds, this current is weakened. On the contrary, under the southerly and southeasterly winds, the current is intensified.

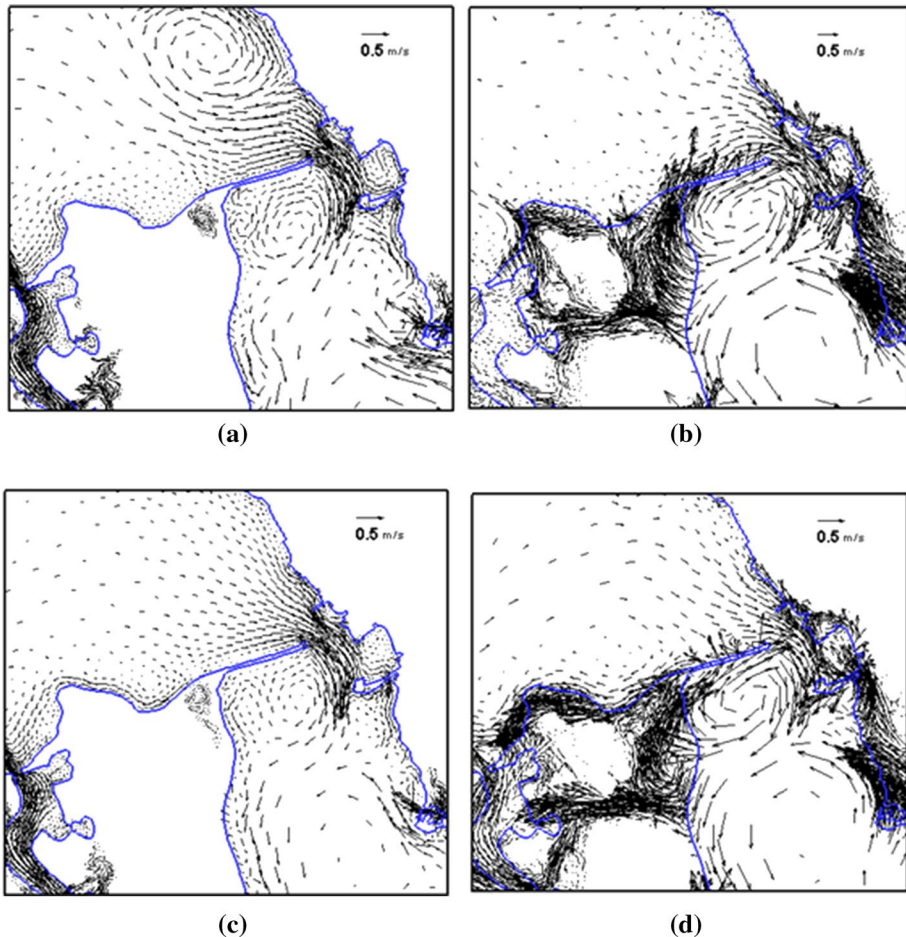


Fig. 10 The velocity vector fields during peak ebbing under southeasterly (a, b) and northeasterly wind (c, d) for the cases with SLRs of 0.0 (left) and 6.0 (right) feet. The vectors denote the current magnitude and direction

Wave fields including the significant wave height and propagation direction under different wind directions are shown in Fig. 12. It demonstrates that waves damp dramatically when they propagate through the mouth of the bay. As aforementioned, the winds with larger fetches such as the southerly, southeasterly and easterly winds tend to drive larger significant wave height at the mouth of the bay than those with small wind fetches such as the northeasterly and northerly winds. Moreover, southerly and easterly winds can cause the wind-induced waves in the bay. The northwesterly wind may cause the waves near the bank and the northerly and northeasterly would not cause any waves in the bay.

The maximum wind-driven surge is shown in Fig. 13. The surge fields for different winds were obtained by subtracting the high tidal level with no wind (Case 20) from that with various winds from Case 1 to 6. It is clear that the northeasterly, easterly, southerly and southeasterly winds drive considerable surges with an average of 0.28 m. Among these, the northeasterly and easterly winds mainly threaten the western coast of the bay and

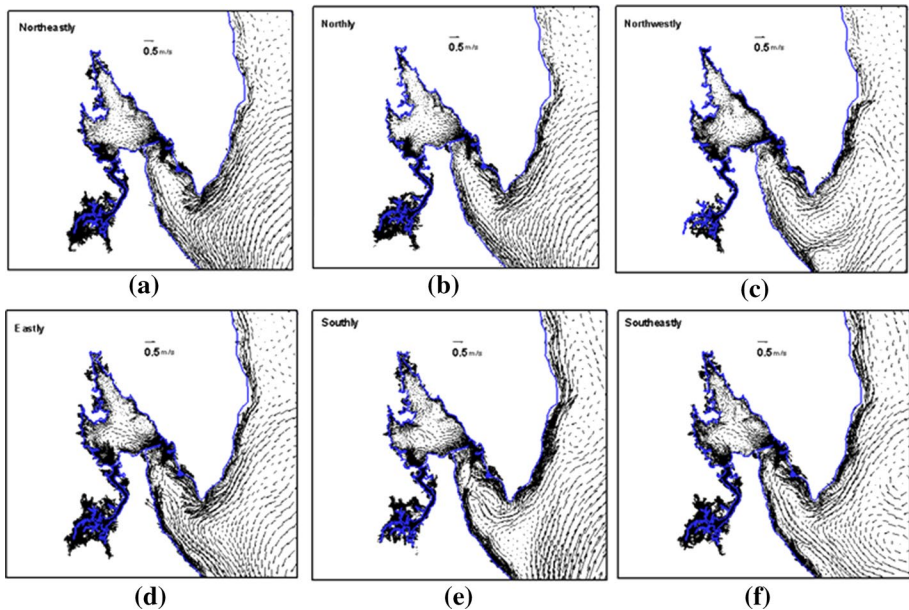


Fig. 11 The velocity vector fields under wind in six direction during peak ebbing

the estuarine areas, and the southerly and southeasterly winds cause surges and inundations around the inner part of the bay. In contrast, the northerly and northwesterly winds drive a large amount of water out of the bay so induce much less surges. Especially the northwesterly wind blows the direction almost opposite to the tide flooding channel into the bay. Therefore, the tide flooding is retained greatly by the wind and almost no positive surge is formed.

5.2 Effect of wave-current interaction

In Scituate Harbor (MA), Beardsley et al. (2013) highlighted the importance of wave-current interaction in the hindcast study of inundation. Here we conducted a couple of experiments (case 20 and 21) to assess the effect of waves on flooding in Apponagansett Bay regardless of wind.

Firstly, we compared the depth-averaged current fields between the cases with and without wave-current interaction. Figure 14 shows that both the flooding and ebbing currents with wave-current interaction are much stronger and more complicated than that without wave-current interaction. With wave-current interaction, at least four eddies are formed and developed with tidal flooding and ebbing near the mouth of the bay. Strong narrow alongshore currents are also formed as the part of these eddies. It is clear that these along shore currents including the northward alongshore current along east coast of Dartmouth in Clarks Cove, is caused mainly by the wave-current interaction and may be intensified or weakened under different winds.

Secondly, while the waves influence current, the tide simultaneously reacts to waves through rising and falling cycles. Figure 15 indicates that more waves would rush and approach the shore during high tide than during low tide. Moreover, the tidal current

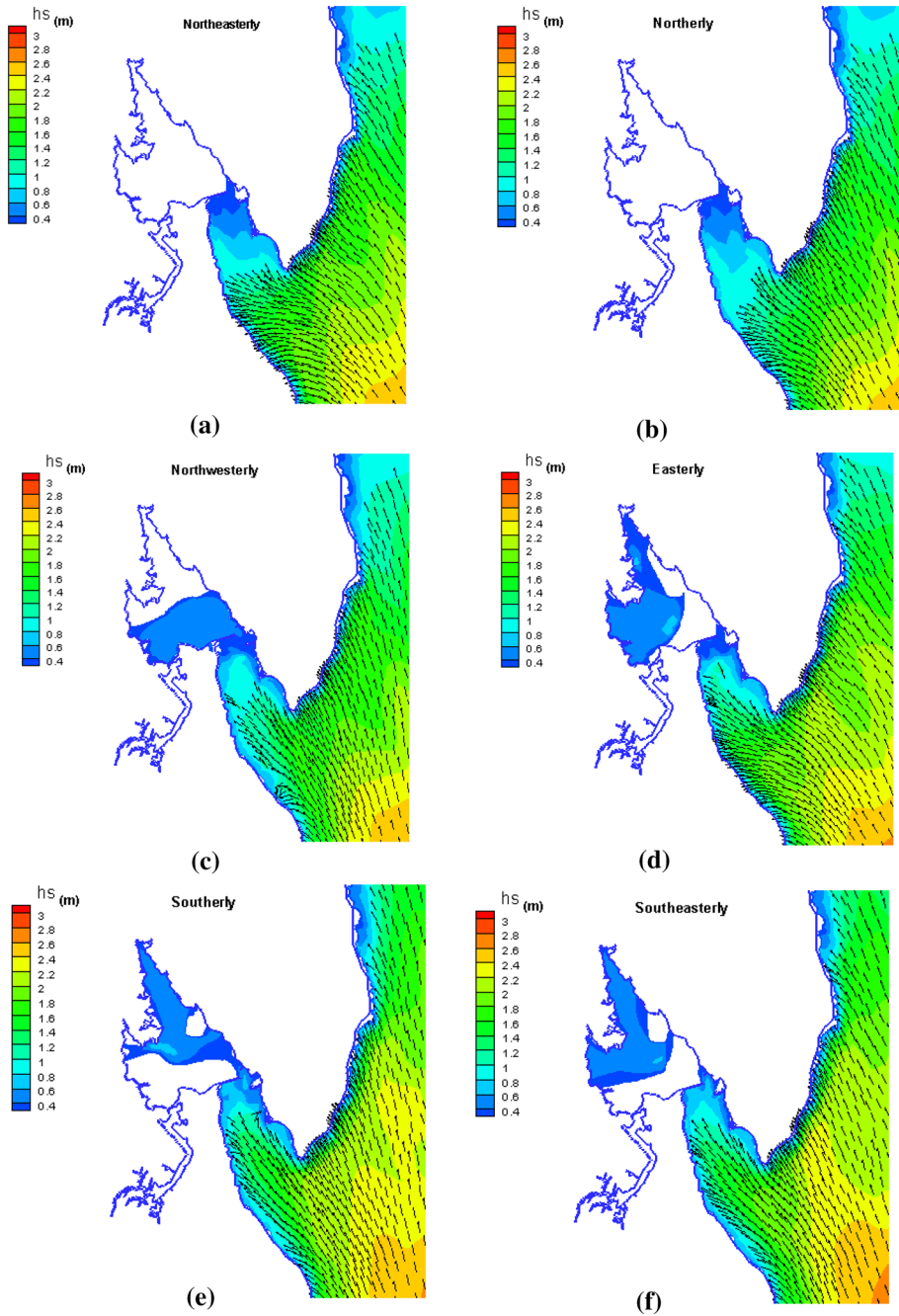


Fig. 12 The wave fields under winds in six directions during peak ebbing, the vectors is wave directions and the color is significant wave height

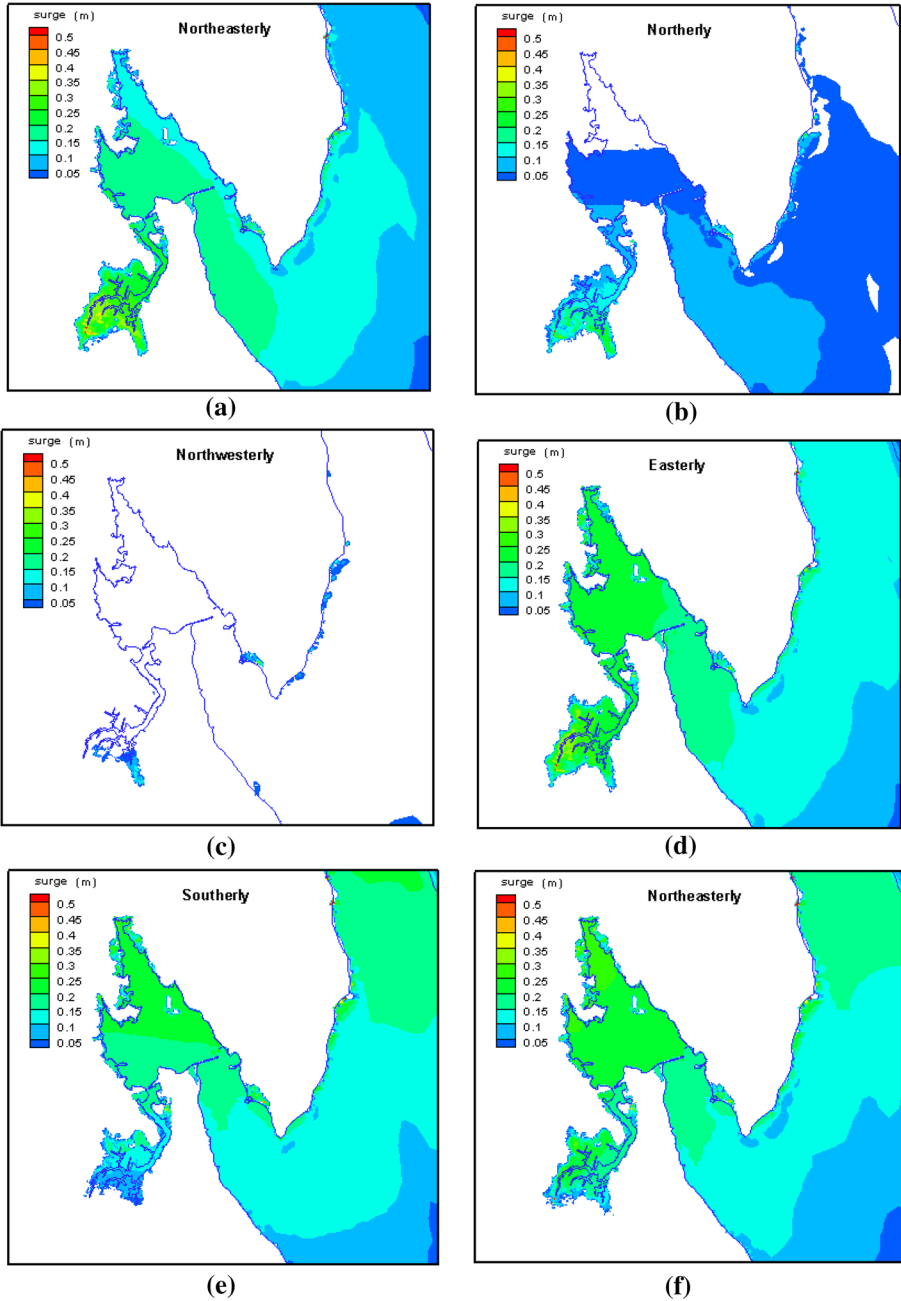


Fig. 13 The surge contour under winds in six directions

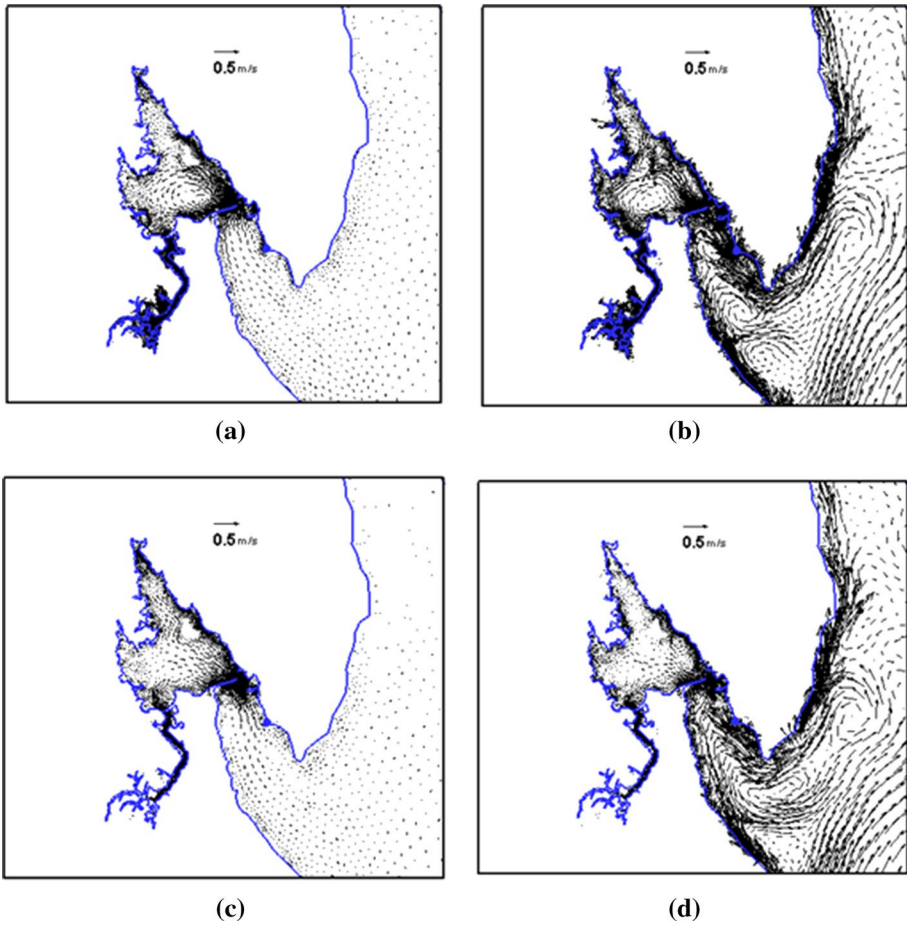


Fig. 14 The velocity vector fields without waves (left) and with waves (right) during peak flooding (upper) and peak ebbing (lower)

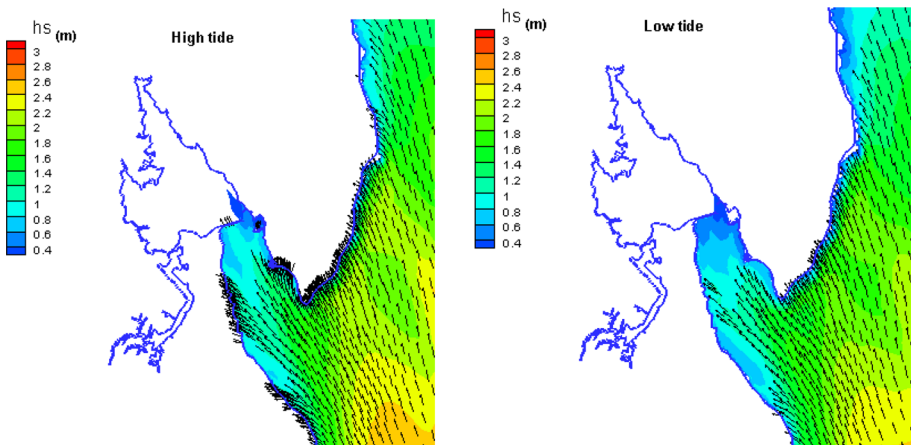


Fig. 15 The wave fields at a level of high tide (left) and low tide (right)

including flooding and ebbing can also react to waves although its influence is much less than that of the tidal level variation. Therefore, bi-directionally interaction between waves and tidal current must be included in simulating flooding inundation in windy coastal region.

Lastly, the wave-induced surge, defined as the level increase driven by the wave radiation stress, is shown in Fig. 16. It demonstrates that the wave-induced surge tends to accumulate in the bay and near the estuarine and coastal regions, and decreases with the distance away from the coast. In Apponagansett Bay (represented by spot A) and Clarks Cove (represented by spot B), the surges vary with the tidal cycles in a nearly inverse relationship, fluctuating around an average of 0.1 m (regardless of the first 12 ramp-up hours). As the sea level approaches high tide, the surges reach downs to the minimum. Otherwise as the sea level approaches the low tide, the surges go up to the maximum.

5.3 Effect of the bank

The local government of the town has spent millions of dollars to build up a bank at the mouth of Apponagansett Bay for protection of waves and surges. Here some extra experiments are conducted to assess the effectiveness the bank. We compared the velocity fields with and without bank at the high tide under different conditions (Fig. 17). It can be seen that the bank blocks a large amount of flooding current into the bay and alter the current pattern significantly at the mouth. Under the normal sea level, the current cannot submerge the bank but flow around it. Therefore, the flow condition in the bay is improved effectively. Under the SLR of 6 ft, though a portion of the flow can get across the bank, the majority of the flow is still blocked outside the bay. Compared to the current, the waves

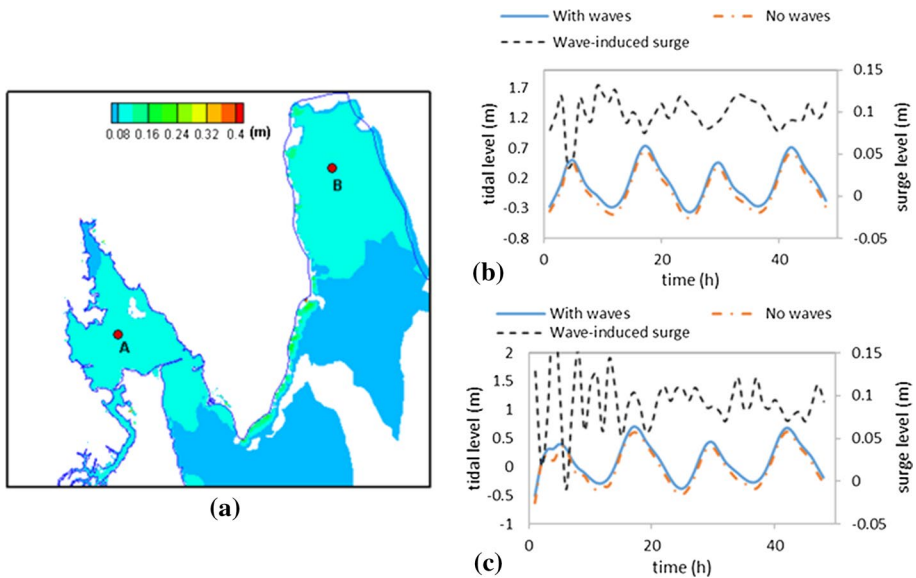


Fig. 16 The wave-induced surge distribution at the 21th hour (a) and the time series of surge (dashed line), corresponding with tidal cycles with waves (solid line) and without waves (dash-dotted line) in spot A (b) and B (c)

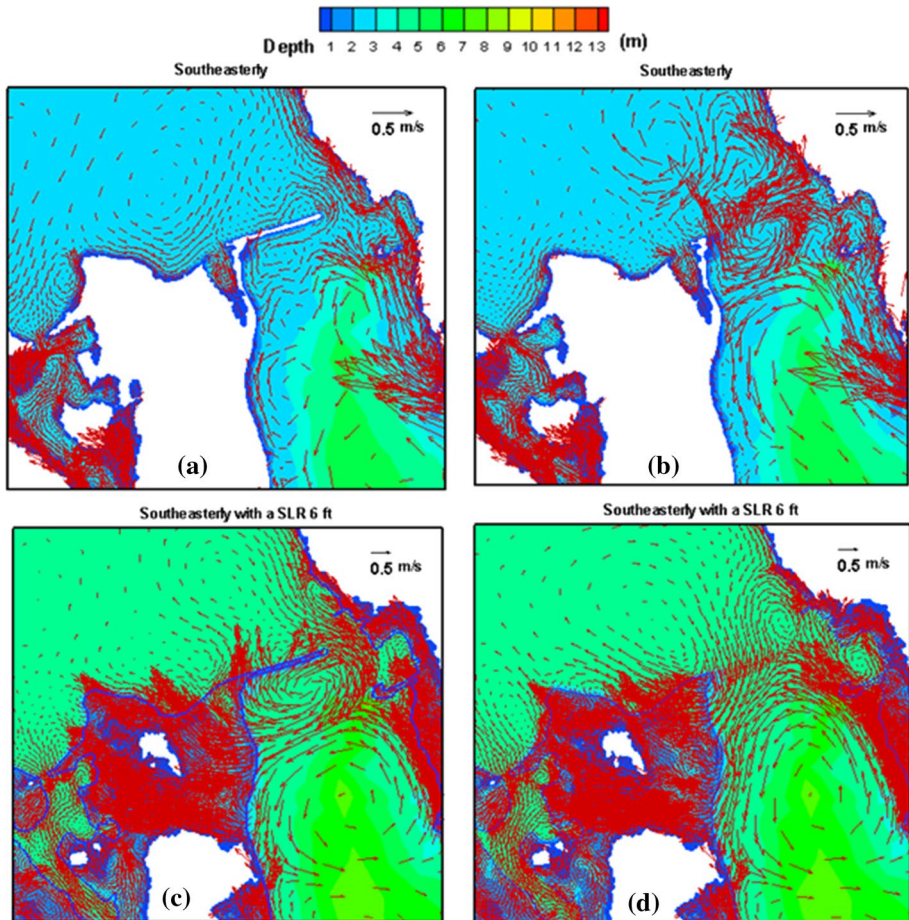


Fig. 17 Current and inundation at the high tide with bank (**a, c**) and without bank (**b, d**). The colors denote the inundation depth

are prevented more effectively by the bank. As shown in Fig. 18, the wave condition in the bay is improved greatly under the cover of the bank both in normal sea level and the SLR of 6ft. For example, under the the southeasterly wind, the bank can reduce the wave height in the bay from nearly 1.8 m to less than 1 m on the SLR of 6ft and from 1.2 m to less than 0.5 m on the normal sea level. Therefore, the bank is an essential protection works in Apponagansett Bay to protect the town.

6 Conclusion

A high-resolution coastal inundation model (DTC-FVCOM) for assessment on potential flooding of Apponagansett Bay and Clarks Cove in Dartmouth Town has been developed, as a subdomain model of the Northeast Coastal Ocean Forest System (NECOFS).

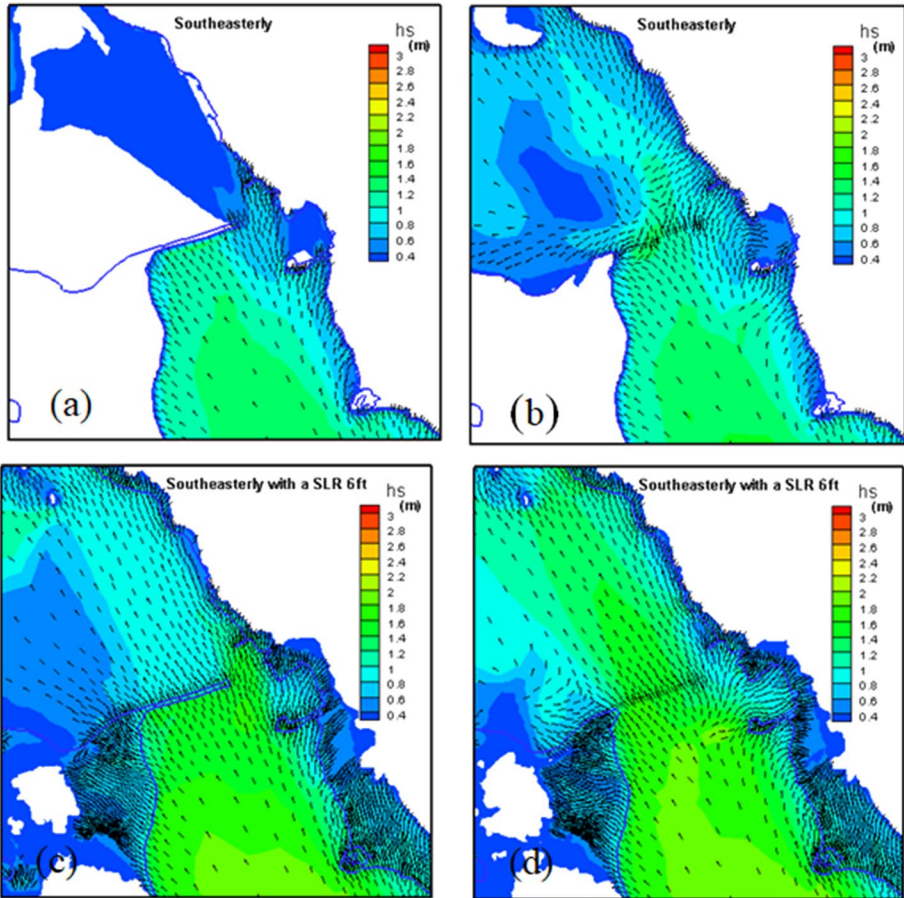


Fig. 18 Waves at the high tide with bank (left) and without bank (right). The colors denote the significant wave height and the arrows denote the wave direction

The Dartmouth inundation model included flooding/drying and wave-current interaction capabilities and could be driven by one-way nesting with NECOFS.

Statistical analysis on wind and tide data was conducted according to simulation result by Weather Research and Forecast (WRF) mesoscale model and NECOFS in the nearshore of Dartmouth town. The extreme wind conditions for 100 return year period and the maximum tidal elevation during a spring tidal cycle was obtained by harmonic and extreme value analysis to impose on the model for simulating the most unfavorable flooding scenarios in Dartmouth Town.

Through a serial of numerical experiments with different SLRs between 1 and 6 feet, the inundation positions and areas, along with the waves and current under the north-easterly and southeasterly winds, were obtained and depicted in the inundation map for demonstrating different inundation areas corresponding to every SLR case. As is expected, climate-change-induced SLRs would significantly enlarge inundation areas with the percentage rate approximately 60% per foot of SLR under the hundred-year

nor'easter storm condition. Meanwhile, waves and current in Apponagansett Bay and Clarks Cove are also enhanced greatly with the SLRs.

Among the driving forces, wind and wave are two critical factors influencing current pattern, surge distribution and inundation regions. In addition, some hydraulic projects such as bank would have significant influence on local current pattern, wave propagation and inundation regions. Numerical experiment results demonstrate that under the same strength, the directions of wind essentially determine the feature of the current, wave and surge distributions. Comparatively, the northeasterly and easterly winds mainly threaten the western coast of the bay and the estuarine areas, and the southerly and southeasterly winds cause more surges and inundation around the inner part and top of the bay. Wave-current interaction can change the current pattern nearshore, including formation of eddies and narrow alongshore currents, greatly enhancing the strength and complexity of the currents near the mouth of the bay. wave-induced surge tends to accumulate in the bay and near the estuary and coastal regions. The bank blocks a large amount of flooding current and waves into the bay and improve the local current and wave conditions effectively at the mouth and inside the bay.

In addition to wind-driven flooding, wave overtopping, which is not considered in this model, may cause significant flooding and property damage along the coast of the bay. The inclusion of the wave overtopping module into the DTC-FVCOM inundation model is the further work. Moreover, the flood risk assessment and damage loss estimate based on various flooding scenarios is under development for further application in flood management and decision-making process.

Acknowledgement The paper was supported by National Natural Science Foundation of China (Grant No. 41771421). In addition, the authors thank the two anonymous reviewers for their helpful suggestions. National Key R & D Program of China 2018YFB0505500, 2018YFB0505502, National Natural Science Foundation of China 41771421.

References

- Beadsley RC, Chen C, Xu Q (2013) Coastal flooding in Scituate (MA): a FVCOM study of the Dec. 27, nor'easter. *J Geophys Res.* <https://doi.org/10.1002/2013JC008862>
- Bernier N, Thompson KR (2006) Predicting the frequency of storm surges and extreme sea levels in the Northwest Atlantic. *J Geophys Res* 111:C10009. <https://doi.org/10.1029/2005JC003168>
- Blake ES, Kimberlain TB, Berg RJ, Cangialosi JP, Beven JL. II, 2013. Hurricane Sandy: October 22–29, 2012, Tropical Cyclone Report, (February 12, 2013), National Hurricane Center, United States National Oceanic and Atmospheric Administration's National Weather Service
- Burchard H (2002) Applied turbulence modeling in marine waters. Springer, Berlin, p 215
- Butman B, Sherwood CR, Dalyander PS (2008) Northeast storms ranked by wind stress and wave-generated bottom stress observed in Massachusetts Bay, 1990–2006. *Cont Shelf Res* 28:1231–1245
- Castelle B, Bonneton P, Senechal N, Dupuis H, Butel R, Michel D (2006) Dynamics of wave-induced currents over an alongshore non-uniform multiple-barred sandy beach on the Aquitanian Coast, France. *Cont Shelf Res* 26:113–131
- Chen C, Liu H, Beardsley R (2003) An unstructured grid, finite-volume, three-dimensional, primitive equations ocean model: application to coastal ocean and estuaries. *J. Atm. & Ocean Tech.* 20(1):159–186
- Chen C, Beardsley RC, Cowles G (2006a) An unstructured grid, finite-volume coastal ocean model (FVCOM) system. *Oceanography* 19:78–89. <https://doi.org/10.5670/oceanog.2006.92>
- Chen C, Cowles G, Beardsley RC (2006b), An unstructured grid, finite-volume coastal ocean model: FVCOM user manual, 2nd ed., Tech. Rep. 06-0602, 315 pp., Univ. of Mass. Dartmouth, Fairhaven
- Chen C, Huang H, Beardsley RC, Xu Q, Limeburner R, Cowles GW, Sun Y, Qi J, Lin H (2011) Tidal dynamics in the Gulf of Maine and New England Shelf: an application of FVCOM. *J Geophys Res.* 116:C12010. <https://doi.org/10.1029/2011JC007054>

- Chen CRC, Beardsley RA, Luettich JJ Jr, Westerink H, Wang W, Perrie Q, Xu AS, Dohahue J, Qi H, Lin L, Zhao P, Kerr Y Meng, Toulany B (2013) IOOS/SURA extratropical storm inundation Testbed: inter-model (ADCIRC, FVCOM and SELFE) comparisons in Scituate, Massachusetts. *J. Geophys Res.* <https://doi.org/10.1002/jgrc.20397>
- Freedman A, 2013 Blizzard of 2013 brings another threat: coastal flooding, Climate Central News published on February 8, 2013
- Hellmer HH, Kauker F, Timmermann R, Determann J, Rae J (2012) Twenty-first-century warming of a large Antarctic ice-shelf cavity by a redirected coastal current. *Nature* 485:225–228
- IPCC 2007: Climate Change 2007: The physical science basis. contribution of working group I to the Fourth Assessment Report of the Intergovernmental Panel on Climate Change [Solomon SD, Qin M, Manning Z, Chen M, Marquis KB, Averyt M Ignore, Miller HL (eds.)]. Cambridge University Press, Cambridge, United Kingdom and New York, NY, USA
- Kobayashi MH, Pereira JMC, Pereira JCF (1999) A conservative finite-volume second-order-accurate projection method on hybrid unstructured grids. *J Comput Phys* 150:40–45
- Lin N, Emanuel K, Oppenheimer M, Vanmarcke E (2012) Physical based assessment of hurricane surge threat under climate change. *Nature Climate Change* 2:462–467. <https://doi.org/10.1038/nclimate1389>
- McCown S 2008 “Perfect Storm” Damage Summary”. National Climatic Data Center. National Oceanic and Atmospheric Administration. <http://www.ncdc.noaa.gov/oa/satellite/satelliteseye/cyclones/pfctstorm91/pfctstdam.html>
- Mellor GL (2003) The three dimensional, current and surface wave equations. *J Phys Oceanogr* 33:1978–1989
- Mellor GL (2008) The depth dependent current and wave interaction equations; a revision. *J Phys Oceanogr* 38:2587–2596
- Mellor GL, Yamada T (1982) Development of a turbulence closure model for geophysical fluid problem. *Rev Geophys Space Phys* 20:851–875
- Nielson C, Apelt C (2003) The application of wave included forces to a two-dimensional finite element long wave hydrodynamic model. *Ocean Eng* 30:1233–1251
- Oey L-Y (2006) An OGCM with movable land–sea boundaries. *Ocean Modell.* 13:176–195
- Peng M, Xie L, Pietrafesa LJ (2006) A numerical study on hurricane-induced storm surge and inundation in Charleston Harbor, South Carolina. *J Geophys Res.* <https://doi.org/10.1029/2004JC002755>
- Pieterzak J, Jakobson JB, Burchard H, Vested HJ, Petersen O (2002) A three-dimensional hydrostatic model for coastal and ocean modeling using a generalized topography following co-ordinate system. *Ocean Model* 4:173–205
- Pritchard HD, Ligtenberg SRM, Fricker HA, Vaughan DG, van den Broeke MR, Padman L (2012) Antarctic ice-sheet loss driven by basal melting of ice shelves. *Nature* 484:502–505
- Qi J, Chen C, Beardsley RC, Perrie W, Lai Z, Cowles G (2009) An unstructured-grid finite-volume surface wave model (FVCOM-SWAVE): implementation, validation and applications. *Ocean Modell.* 28:153–166
- Rahmstorf S (2010) A new view on sea level rise. *Nature* 4:44–45
- Sallenger AH Jr, Doran KS, Howd PA (2012) Hotspot of accelerated sea-level rise on the Atlantic coast of North America. *Nat Clim Change* 2:884–888. <https://doi.org/10.1038/nclimate1597>
- Smagorinsky J (1963) General circulation experiments with the primitive equations, I. The basic experiment. *Monthly Weather Rev* 91:99–164
- USA Today-30-October 2012. Sandy leaves millions without power: 15 dead
- Vallee DR, Dion MR 2005. Hurricane Bob, Boston, MA National Weather Service, Retrieved 2011-07-12
- Warner JC, Sherwood CR, Signell RP, Harris CK, Arango HG (2008) Development of a three-dimensional, regional, coupled wave, current, and sediment-transport model. *Comput Geosci* 34:1284–1306
- Xie L, Liu H, Peng M (2008) The effect of wave–current interactions on the storm surge and inundation in Charleston Harbor during Hurricane Hugo 1989. *Ocean Modell.* 20:252–269
- Zhang KQ, Douglas BC, Leatherman SP (2000) Twentieth-century storm activity along the US east coast. *J Clim* 13(10):1748–1761